Journal of Power Sources 275 (2015) 234–242

Contents lists available at ScienceDirect

Journal of Power Sources

journal homepage: www.elsevier.com/locate/jpowsour

Prospects for reducing the processing cost of lithium ion batteries

David L. Wood III *, Jianlin Li, Claus Daniel

Oak Ridge National Laboratory, Energy & Transportation Science Division, One Bethel Valley Road, P.O. Box 2008, Oak Ridge, TN 37831, USA

HIGHLIGHTS

- A comprehensive cost study on lithium-ion electrode processing is reported.
- Advanced electrode processing can save up to $111/kWh-usable.
- Reduced SEI-layer formation time can save an additional $22/kWh-usable.
- These processing technologies are amenable to any anode or cathode chemistry.
- Capital cost savings realized and cell processing bottlenecks addressed.

GRAPHICAL ABSTRACT

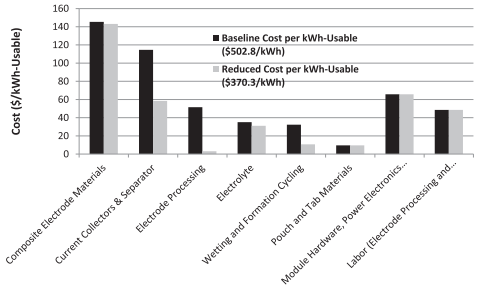

ARTICLE INFO

Article history:
Received 26 August 2014
Received in revised form
4 November 2014
Accepted 5 November 2014
Available online 6 November 2014

Keywords:
Lithium-ion battery
Cost reduction study
Electrode processing
Aqueous colloidal chemistry
Thick electrodes
Formation cycle

ABSTRACT

A detailed processing cost breakdown is given for lithium-ion battery (LIB) electrodes, which focuses on: 1) elimination of toxic, costly *N*-methylpyrrolidone (NMP) dispersion chemistry; 2) doubling the thicknesses of the anode and cathode to raise energy density; and 3) reduction of the anode electrolyte wetting and SEI-layer formation time. These processing cost reduction technologies generically adaptable to any anode or cathode cell chemistry and are being implemented at ORNL. This paper shows step by step how these cost savings can be realized in existing or new LIB manufacturing plants using a baseline case of thin (power) electrodes produced with NMP processing and a standard 10–14-day wetting and formation process. In particular, it is shown that aqueous electrode processing can cut the electrode processing cost and energy consumption by an order of magnitude. Doubling the thickness of the electrodes allows for using half of the inactive current collectors and separators, contributing even further to the processing cost savings. Finally wetting and SEI-layer formation cost savings are discussed in the context of a protocol with significantly reduced time. These three benefits collectively offer the possibility of reducing LIB pack cost from $502.8 kW h^{-1}-usable to $370.3 kW h^{-1}-usable, a savings of $132.5/kWh (or 26.4%).

1. Introduction

For lithium ion batteries (LIBs) to take their place in widespread commercialization of hybrid electric vehicles (HEVs), plug-in hybrid electric vehicles (PHEVs), and full electric vehicles (EVs), system cost must still be reduced by 3–4× to about $125 kW h^{-1}. [1] Three important ways to achieve significant system cost reduction are to: 1) lower the electrode processing cost associated with the costly organic solvent and primary solvent drying time; 2) substantially increase the electrode thicknesses to ~2× the current "power" levels (to 3.5–4.5 mA h/cm^2) while preserving power density; and 3) reduce the formation time associated with the anode solid electrolyte interface (SEI) layer. These lithium-ion cell fabrication steps contribute significantly to the current overall pack cost of $400–600 kW h^{-1} and will be the focus of the discussion

* Corresponding author.
E-mail address: wooddl@ornl.gov (D.L. Wood).

http://dx.doi.org/10.1016/j.jpowsour.2014.11.019

and associated calculations in this paper. Formulation, coating thickness, drying, and NMP recovery aspects will be considered with respect to electrode processing cost, and wetting and low-rate cycling will be addressed with respect to cell formation time. A cost assessment approach (at low volume) can be employed to identify potential links between electrode processing aides, process energy consumption, and LIB pack cost.

There are two recent, well-known LIB cost studies from Argonne National Laboratory (ANL) [2] and TIAX, LLC, [3] but these studies consider the entire cell production process without sufficient granularity on individual electrode processing and cell fabrication steps. These cost models are also heavy on contributions from materials, labor, capital equipment, and performance without detailed consideration of process energy requirements. The ANL "BatPaC" model takes a comprehensive approach to determining 40-Ah pouch cell and component masses and dimensions, cost *vs*. performance characteristics, and pack-level performance with the modeled cell chemistries. The goal of the work was to design specific LIBs and the required manufacturing facility based on user defined performance specifications for an assumed cell, module, and pack format. It focuses primarily on performance tradeoffs, pack design, and plant layout features [2]. The TIAX model took a comprehensive approach to examining the manufacturing costs of 5.5-kWh-rated packs for PHEVs based on 18650 cells, where the major emphasis was on material selection tradeoffs and power/energy optimization, and capacity fade effects. The model did consider the processing cost effect of electrode thicknesses and gave a cost breakdown of key electrode processing steps [3], though it was not completely evident how these processing steps contributed to the total LIB pack cost. This paper will build upon the foundational work of ANL and TIAX by giving an in-depth review of the energy consumption associated with electrode processing and formation cycling, two particularly costly elements of lithium-ion cell production, and how manufacturing cost savings could be realized.

1.1. Aqueous processing of LIB electrodes

Purchasing and handling the *N*-methylpyrrolidone (NMP) solvent used in much of the electrode formulation and coating steps adds significant manufacturing cost to the LIB pack. More processing energy (heated air flow) is required to remove NMP during drying of the electrode coatings than other solvents (such as water and lower alcohols) with much lower boiling points and higher vapor pressures. In addition, it must be recovered as a volatile organic compound (VOC). NMP recovery involves significant capital expense since multiple condensers or distillation towers are needed, and its use adds to the cost of the coating line equipment in making it explosion proof. A less expensive manufacturing approach is to use water-based "aqueous processing" to make LIBs, taking advantage of advanced colloidal chemistry and formulation science.

Although colloidal approaches have been utilized for many years in ceramic slurry and dispersion development, [4–9] there has been little published in this area with respect to LIBs until recently, which coincides with an increased interest in switching from organic to aqueous systems. The emphasis has been primarily on the dispersion of $LiFePO_4$, utilizing a variety of dispersants to control agglomeration and wetting improvement of the dispersions on current-collector substrates [10–23]. As the complexity of LIB dispersions grows with the addition of novel conductive additives and more diverse powder chemistries and morphologies, the challenge has become control of the interparticle forces between like and un-like surfaces.

Processing of LIB electrodes with water is gaining traction worldwide, as the environmental and safety concerns associated with NMP handling are rapidly growing. For example, in Japan and South Korea anodes are almost exclusively produced using water based chemistry, and there is great interest in Germany in eliminating NMP altogether. Prominent U.S. manufacturers such as A123 Systems and Johnson Controls are developing the technology as well. However, implementation of aqueous processing for the cathode remains difficult because less is known about how to disperse these materials successfully in water. Several problems are introduced such as agglomeration due to strong interaction between particles and inferior wetting of the cathode dispersion onto the Al current collector. Li et al. has made substantial progress in solving these two problems [23,24], and has also introduced the methods of multicomponent dispersants for the active material and acetylene black conductive additive and order of addition (mixing sequence) optimization to maximize $LiFePO_4$ cathode performance [25,26]. A third issue is how to remove enough residual water from the coated electrodes. Wood has also addressed this problem by optimizing the primary drying (*i.e*. drying immediately after coating) process parameters, and demonstrated residual water content in a $LiFePO_4$ cathode well below the industry standard of less than ~500 ppm [27]. In fact, the notion that aqueous electrode processing will substantially ***save*** on primary drying energy costs will be advanced here.

1.2. Increasing LIB electrode thicknesses

Cathode thicknesses, which currently limit the cell specific capacity and energy density and indirectly add to cell cost, should also be significantly increased, so fewer inactive components (current collectors and separators) are required per cell. Active-material specific capacities for LIBs are relatively high, but the cells suffer lower specific capacity due to the amount of inactive material such as current-collector foil and separator, which limit practical cell energy density to about 200–225 Wh kg^{-1}. For example, the typical capacity of a graphite/$LiNi_xMn_yCo_{1-x-y}O_2$ (NMC) cell is about 150 mAh g^{-1} based on the cathode active material mass. When factoring in the anode active material and inactive component masses (current collector foils, separators, electrode binder, and conductive additive), this value drops to about 60 mAh g^{-1} (60% reduction).

One way to address this limitation is to increase the cathode coating thickness while balancing it with a thicker anode, which raises unit-cell energy density while simultaneously lowering battery-pack cost. When this modification is made, however, the cathode kinetics limit cell capacity, and an optimized cathode architecture (materials and structure) must be implemented. From a processing standpoint, this change has been considered by industry for quite some time; however, implementation has not occurred because thick cathodes are not compatible with current inactive material compositions and dispersion processing. Practical limitations of the coating process such as breakdown of coating integrity (particle cohesion), delamination of coating from current collector foil (particle adhesion), and excessive flaking as the web traverses the coating line impose a maximum calendered cathode thickness of about 100 μm (for a single-sided coating).

By doubling the cathode thickness to ~200 μm in a graphite/NMC cell (along with a balanced anode thickness), capacity would increase by ~17% from about 60 mAh g^{-1} to 70 mAh g^{-1} (total cell mass basis), reducing cell cost considerably. In addition, the amount of geometric surface area (current-collector, electrode, and interfacial contact area) that would need to be managed during electrode processing and cell assembly would be reduced by 2×.

1.3. SEI layer formation and electrode wetting

The process of formation cycling refers to the electrochemical side reactions involved with creating an electronically passive film on the anode active material, for instance graphite, known as the solid electrolyte interface (SEI) layer. This interfacial layer is formed during the first several charge–discharge cycles primarily by the reaction of electrolyte components with graphite at reducing potentials approaching the standard reduction potential of lithium metal (−3.045 V *vs.* SHE), and it plays a protective role by preventing the graphite from undergoing subsequent reactions with electrons, electrolyte solvent, and salt [28]. An ideal SEI layer should be thin, minimally porous, electrochemically inert, electronically resistive, and ionically conductive.

In order to form stable SEI layers that cover all of the anode and cathode surface area and to ensure good lithium ion conductivity and rate capability, there must be complete wetting of the electrode and separator pores. In practice, however, there are substantial barriers to wetting – the separator pores (polyethylene surface energy is 35–36 mN m^{-1} and polypropylene surface energy is only 30.1 mN m^{-1}), the electrode binder, and the conductive carbon black additive. A period of ~12–24 h under vacuum is required to achieve adequate wetting during the cumbersome electrolyte filling process of cell assembly, and it still leaves a substantial fraction of the smallest pore volume unwetted.

Formation cycling is performed after a lithium ion cell has been constructed, tap charged, and rested for ~24 h, and it has a significant economic impact on lithium ion battery manufacturing. The formation process requires that battery producers install many thousands of cycling stations to complete the process, which results in a heavy capital equipment investment, a much larger plant size, and a considerable manufacturing bottleneck. The irreversible capacity loss associated with anode SEI formation involves the consumption of lithium inventory from the fresh cathode ($LiCoO_2$, $LiMn_2O_4$, NMC, $LiFePO_4$, *etc.*), resulting in a diminished battery lifetime. However, without the protective SEI layer, battery lifetime would render LIBs unusable.

The formation process is generally thought to occur in two successive stages, with the first stage involving formation of a highly ionically resistive SEI layer at higher anode potentials (>0.25 V *vs.* Li/Li^+). The second stage involves simultaneous intercalation of lithium into the graphite at potentials <0.25 V *vs.* Li/Li^+ where the SEI layer is converted to a highly ionically conductive film [29]. Fong et al. showed that the second stage involving the initial intercalation of lithium into graphite does not occur without the proper decomposition of electrolyte solvent and a sufficient coverage of SEI film [30]. There are three primary methods of formation cycling, which consist of a two-step current-charge formation, [31] pulse formation, [32] or the aging process at elevated temperature [33]. In industry, complex and proprietary combinations of these methods are used.

Electrode wettability plays a critical role in SEI layer formation [34]. After electrodes are coated and dried, they are usually calendered at high pressure to compact the composite structure, thus improving the energy density of the electrode layer. However, the electrode porosity is correspondingly reduced to only 30–35%, which has a significant impact on the pore-size distribution and the related wetting of the electrolyte [34]. The majority of electrode surface area in a calendered anode corresponds to pores that are <100 nm, and for the electrolyte to fill these small pores, the surface energy of the electrode should be much higher than the surface tension of the electrolyte.

The steps of electrode wetting and formation cycling also add significant processing energy cost per kWh of usable energy, which is sometimes improperly estimated in LIB pack cost calculations. Furthermore, the wetting and formation steps are an unacceptable process time bottleneck and add substantial capital cost to a LIB production plant.

1.4. Electrode processing cost modeling motivation

Since LIB pack costs must still be reduced ~3–4× to achieve the DOE cost target, development of a robust cost reduction strategy is of paramount interest. Electrode processing is a key element of this strategy, and it can be implemented on the front end of a longer-term pathway. Because of the potential of significant cost savings associated with each of the three electrode processing steps discussed above, it is useful to understand the sources of the savings from a technical standpoint. Detailed cost reduction calculations will be presented in the next two sections highlighting: 1) electrode processing cost and energy consumption related to solvent type, dispersion solids loading, drying temperature, air flow rate, and drying time; 2) effect of electrode thickness on cost as related to the amount of inactive current collectors and separators; and 3) heating and electricity cost of electrolyte wetting and SEI-layer formation.

2. Electrode processing cost calculations

2.1. Major simplifying assumptions in the cost modeling

Several key assumptions were made to assist in the overall cost calculations presented in the subsequent subsections (2.2–2.4). They are as follows:

- Low-volume (<1000 battery packs) production of 52-Ah automotive "power cells" was assumed. (This approach is different than the ANL and TIAX models, which considered higher volume manufacturing, but what is more important here is the relative cost savings percentages that would be realized at any production volume.)
- A single electrode size of 21 cm × 24 cm was used for the total electrode area per cell even though in practice the anode and cathode have slightly different geometries.
- Standard current collector thicknesses of 9 μm for the anode Cu foil and 15 μm for the cathode Al foil were assumed for calculating the electrode parameters such as thickness, porosity, etc.
- An air flow rate of 8000 ft^3 min^{-1} was assumed for NMP drying at industrial scale.
- A cost savings of 80% ($1.1/lb *vs.* $5.5/lb) was assumed for non-PVDF water-soluble binders such as carboxymethylcellulose (CMC), styrene butadiene rubber (SBR), fluorine acrylic hybrid latex, etc. For example, PVDF dispersion costs are estimated at $8.6–10.5/lb *vs.* only $0.5–1.4/kg for CMC.
- A much lower solvent-drying temperature for DI water of 90 °C and air flow rate of 4000 ft^3 min^{-1} was assumed for water-based electrode processing.
- The evaporation rate of water from the wet coating was assumed to be 2 × (4×10^{-3} g min^{-1} cm^{-2}) that used for NMP due to the much lower boiling point, much higher vapor pressure of water, and significantly lower heat of vaporization.
- A series of four barometric condensers was used to estimate the cost of NMP recovery.

2.2. Processing baseline calculations

The baseline for this series of calculations is NMP/polyvinylidene fluoride (PVDF) processed electrodes with standard coating thicknesses. A 52-Ah ***pouch*** cell with 21 cm × 24 cm

electrode dimensions was used for all calculations. The cell had 36 double-sided anodes, 2 single-sided anodes, and 37 double sided cathodes, or 74 unit cells. All pouch cell and electrode materials of construction, as well as the associated costs, were held constant for both cases. The cell design selected for this work was based on an actual industrial "power cell" for transportation applications with a graphite anode and a $LiNi_xMn_yCo_{1-x-y}O_2$ (NMC) cathode (see Table 1 for electrode and separator details). Based on assumed anode and cathode specific capacities of 325 and 150 mA h/g, respectively, and a N:P ratio of 1.1, coating areal weights were 5.24 and 10.33 mg cm^{-2} for the anode and cathode (single-sided coating), respectively, and areal capacities were 1.53 and 1.39 mAh cm^{-2} for the anode and cathode, respectively. The ratios of active material to binder to conductive additive were assumed to be 90:5:5 wt% for both electrodes. Electrode thicknesses were estimated at 45 μm and 50 μm for the anode and cathode, respectively, which yielded electrode bulk densities of 1.2 and 2.1 g cm^{-3} for the anode and cathode, respectively. Based on the bulk densities, electrode porosities were estimated at about 44% for the anode and 49% for the cathode for calculating the electrolyte volume needed. Separator porosity was estimated at 39%, and the thickness was assumed to be 25 μm. For the baseline, 204 mL of electrolyte was required to fill the separator and electrode pores.

Taking 90 wt% of active material for each electrode along with 5 wt% each of PVDF binder and conductive carbon additive, 580.7 g of total electrode mass is obtained. Using an anode and cathode dispersion solids loading of 45 wt%, 709.8 g of NMP is obtained. At a bulk-quantity price of \$1.25 L^{-1} for NMP (see Table 2 for the cost estimates of individual cell materials), the normalized cost for NMP results in \$0.017 Ah^{-1}. As for the PVDF binder, 29.0 g are required for these formulations, and at a bulk price of \$5.50 lb^{-1}, the normalized cost for PVDF is \$0.007 Ah^{-1}. This yields a NMP/PVDF material cost of \$0.024 Ah^{-1}.

A drying temperature for NMP of 150 °C at an air flow rate of 8000 ft^3 min^{-1} was assumed, which is typical for industrial scale slot-die coaters. This flow rate is also estimated from knowledge of the exhaust requirements of the ORNL slot-die pilot coating line. At ORNL, 1200 ft^3 min^{-1} is used for 12-inch wide, single-sided coatings. In a LIB manufacturing plant, the coating widths are several feet wide and coated on both sides of the current collector.

Table 1
Electrode parameters for baseline cost reduction calculations (N/P ratio was set to 1.1); cell chemistry was a graphite anode and $LiNi_xMn_yCo_{1-x-y}O_2$ (NMC) cathode.

Parameter	Value
Anode graphite specific capacity	325 mA h/g
Anode areal capacity	1.53 mA h/cm^2
Anode areal weight	5.24 mg/cm^2
Anode active material fraction	90 wt%
Anode carbon black fraction	5 wt%
Anode PVDF binder fraction	5 wt%
Anode thickness	45 μm
Anode bulk density	1.2 g/cm^3
Estimated anode porosity	44%
Cathode NMC specific capacity	150 mA h/g
Cathode areal capacity	1.39 mA h/cm^2
Cathode areal weight	10.33 mg/cm^2
Cathode active material fraction	90 wt%
Cathode carbon black fraction	5 wt%
Cathode PVDF binder fraction	5 wt%
Cathode thickness	50 μm
Cathode bulk density	2.1 g/cm^3
Estimated cathode porosity	49%
Separator porosity	39%
Separator bulk density	0.55 g/cm^3
Separator thickness	25 μm
Separator areal weight	1.4 mg/cm^2

Table 2
Pouch cell, electrode materials, solvent, and electrolyte cost assumptions for Thick NMP Case calculations.

Material	Cost
Anode graphite	\$9/lb
Cathode NMC	\$19/lb
Carbon black conductive additive	\$2.5/lb
PVDF binder	\$5.5/lb
NMP solvent	\$1.25/L
Copper foil	\$7.5/lb
Aluminum foil/tab	\$1.5/lb
Separator	\$3/m^2
Nickel tab	\$7.8/lb
Pouch material	\$5/m^2
Electrolyte	\$22/L

The NMP evaporation rate was based on a drying experiment discussed elsewhere, [35] in which the rate of weight loss of NMP was measured from a $LiCoO_2$ based electrode coating with PVDF as the binder where the temperature and linear velocity of the air was 100 °C and 2.2 m s^{-1} respectively. At these conditions, the thermogravimetric measurements revealed a maximum NMP evaporation rate of 5×10^{-4} g min^{-1} cm^{-2} in the pure solvent evaporation zone of the drying curve. Since the temperature used in the calculations here is much higher (i.e. 150 °C) and the linear velocity is also higher at ~5–6 m/s (8000 ft^3 min^{-1} through a ~3-ft diameter pipe), an evaporation rate 4 × higher was used, i.e., 2×10^{-3} g min^{-1} cm^{-2}. Based on these air flow rate conditions, a heat input rate for ambient supply air of 23,827 kJ min^{-1}, or 397 kW, is required. Using the NMP evaporation rate of 2×10^{-3} g min^{-1} cm^{-2} and a total-cell electrode active area of 7.46 m^2 (equivalent to all double-sided anodes and cathodes plus two single-sided anodes in a 21 cm × 24 cm cell), a total evaporation rate of 2.49 g-NMP s^{-1} is calculated. From the total amount of solvent required of 709.8 g for a 52-Ah cell, an NMP drying time of 0.079 h (4.76 min) can be estimated, which corresponds to 31.5 kW h of energy consumption for drying, or \$0.061/Ah for the drying cost (assuming \$0.10 kW h^{-1} average energy price).

A basic condenser process was assumed to obtain a conservative estimate of the cost of NMP recovery. A series of four barometric condensers sized 35 ft tall and 15 ft diameter were used for the calculations in which the hot air containing the dissolved NMP is exchanged in "bottom-up" fashion with atomized, chilled water entering from the top of the condenser towers. In a real process, vacuum distillation or surface condensation with adsorption would likely be used. These processes are typically more expensive than barometric condensation, so the following calculation gives a minimum cost associated with NMP solvent recovery. Coolant water inlet and exit temperatures of 5 °C and 35 °C were assumed, respectively. Using the enthalpy of 150 °C air of 425 J g^{-1} and the cooling water heat capacity of 4.189 J g^{-1} K^{-1}, the rate of cooling water can be calculated according to Equation (1) below:

$$\frac{W}{V} = \frac{H_S - c_p(T_2 - 273.3)}{c_p(T_2 - T_1)} \quad (1)$$

at 2.22 g-water g-air^{-1}, where W is the flow rate of cooling water, V is the air flow rate, H_S is the enthalpy of steam, c_p is the heat capacity of the cooling water, T_2 is the warm water temperature, and T_1 is the inlet cooling water temperature [36]. For a four stage condenser process, this corresponds to 27.9 kg-water s^{-1} and a heat removal rate from the supply water (to achieve 35 °C outlet

temperature) of 1990 kW. To determine the energy consumption of this condensation process, the residence time of the NMP-containing air stream can be utilized, which is simply the total condenser volume divided by the volumetric flow rate of air. The air residence time was found to be 0.013 h (47 s). Taking the heat removal rate multiplied by the residence time yields 25.6 kW h, or a processing cost of \$0.049 Ah^{-1} (assuming \$0.10 kW h^{-1} average energy price). Taking the sum of the NMP and PVDF materials, NMP drying, and NMP condensation costs, a total normalized cost of \$0.134 Ah^{-1} (\$38.3 kW h^{-1}) is obtained. Table 3 summarizes the ***cell*** cost contributions for the baseline on a ***total-kWh*** basis, and Table 4 summarizes the total pack cost on both a total-kWh and usable-kWh basis. In this analysis, the main focus is on the top rows of Table 4—i.e. costs such as pack construction and labor were taken from other sources [1,2] and are included only for obtaining a full pack cost for comparison to other cost models.

2.3. Aqueous processing calculations

A much lower solvent-drying temperature for DI water of 90 °C and air flow rate of 4000 ft^3 min^{-1} (assumed as ½ the flow rate needed for NMP processing) may be used for water-based electrode processing. The evaporation rate of water from the wet coating was assumed to be $2 \times (4 \times 10^{-3}$ g min^{-1} $cm^{-2})$ that used for NMP due to the much lower boiling point, much higher vapor pressure of water, and significantly lower heat of vaporization – a conservative estimate. The boiling point at ambient conditions of NMP is 204.3 °C, as opposed to only 100.0 °C for water. In addition, the vapor pressure at 40 °C of NMP is only 1.0 mmHg, as opposed to 55.3 mmHg for water – well over an order of magnitude difference in volatility. Finally, the heat of vaporization at 100 °C for NMP is 50.6 kJ mol^{-1} *vs.* only 40.7 kJ mol^{-1} for water.

Based on these air flow rate conditions and water evaporation rate, a heat input rate for ambient supply air of 7912 kJ min^{-1}, or 120 kW, is required. Using the DI water evaporation rate of 4×10^{-3} g min^{-1} cm^{-2} and the same electrode active area of 7.46 m^2, a total evaporation rate of 4.97 g-water s^{-1} is calculated. From the total amount of solvent required of 387 g (based on 60 wt % solids loading in the electrode dispersions) for 52-Ah cell, a DI water drying time of 0.022 h (1.30 min, which is 3.7× faster than the drying time associated with NMP at half the flow rate of drying air) is calculated. This time corresponds to 2.60 kW h of energy consumption for preliminary drying (obtained by multiplying drying heat input rate of 120.3 kW by 0.022 h), or \$0.0050 Ah^{-1} for the drying cost. Taking the sum of the DI water and water-soluble binder materials (\$0.015/L and \$1.1/lb, respectively) and drying costs (solvent recovery costs are eliminated), a total normalized cost of \$0.0051 Ah^{-1} (\$1.46 kW h^{-1}) is obtained. This value compares quite favorably to the \$38.3 kW h^{-1} for NMP-based processing obtained at the end of Section 2.2.

Table 4
LIB pack cost contributions for baseline electrode processing case (cost per kWh-usable energy assumes a 70% depth-of-discharge for cycling).

Cost component	Cost per kWh-total (\$/kWh)	Cost per kWh-usable (\$/kWh)
Composite electrode materials	101.7	145.3
Current collectors & separator	80.2	114.6
Electrode processing	36.1	51.6
Electrolyte	24.6	35.1
Wetting and formation cycling	22.6	32.3
Pouch and tab materials	6.7	9.6
Module hardware, power electronics & pack cooling [1]	46	65.7
Labor (electrode processing and cell/pack construction) [2]	34	48.6
Total	351.9	502.8

2.4. Cost benefits of thicker cathodes (thick aqueous case)

For the thick aqueous case, both the anode and cathode thicknesses were doubled to 90 μm (10.8 mg cm^{-2} areal loading) for the anode and 100 μm (21.2 mg cm^{-2} areal loading) for the cathode, so the number of cells reduces to 17.5 double-sided anodes, 2 single-sided anodes, and 18.5 double-sided cathodes (37 unit cells). In addition, the amount of total electrode area drops to 3.73 m^2. All other electrode parameters (active materials, binder, bulk density, material constituent wt fractions, etc.) were held constant relative to the baseline. Essentially this change means that approximately half the number of Al and Cu current collectors and separators may be used in the 52-Ah cells. Table 5 shows how the cost breakdown changes for the cell cost per total kWh when both the changes to aqueous processing and thick electrodes are implemented. It is seen that the cell production cost is reduced from \$249.36 kW h^{-1}-total (in Table 3) to \$171.78 kW h^{-1}-total (in Table 5).

Over a 90% cost reduction can be achieved with the combination of 1) less expensive binder and solvent materials and 2) less expensive electrode processing steps (coating, drying, and solvent recovery) in switching from a NMP-based colloidal chemistry to an aqueous one. An additional ~50% reduction in the cost of current collector foils and separators can be realized by doubling electrode thicknesses. The cumulative savings in these electrode processing, inactive cell component (separator, current collectors, and binder), and electrolyte costs is \$77.6 kW h^{-1}-total when comparing Table 3

Table 3
Breakdown of cost by \$/Ah-Total and \$/kWh-Total (assuming an average cell voltage of 3.5 V) for baseline (NMP/PVDF processing at standard electrode thicknesses).[a]

Thin NMP case	Breakdown	\$/Ah	\$/kWh
Cu foil	5.6%	0.0491	14.02
Anode	8.1%	0.0704	20.12
Separator	26.0%	0.2268	64.80
Cathode	32.7%	0.2855	81.58
Al Foil	0.5%	0.0048	1.37
Pouch material	2.2%	0.0191	5.46
Tab materials	0.5%	0.0045	1.28
Solvent	1.9%	0.0166	4.73
Solvent drying	6.9%	0.0606	17.30
Solvent recovery	5.7%	0.0493	14.09
Electrolyte	9.9%	0.0861	24.61
Total	100.0%	0.8728	249.36

[a] Costs are for cell construction only and do not include SEI formation step and pack assembly costs.

Table 5
Breakdown of cost by \$/Ah-Total and \$/kWh-Total (assuming an average cell voltage of 3.5 V) for thick aqueous case (water based processing with 2× thicker electrodes).[a]

Thick aqueous case	Breakdown	\$/Ah	\$/kWh
Cu foil	4.1%	0.0245	7.01
Anode	11.5%	0.0686	19.60
Separator	19.4%	0.1163	33.23
Cathode	47.1%	0.2819	80.55
Al foil	0.4%	0.0023	0.67
Pouch material	3.2%	0.0191	5.46
Tab materials	0.7%	0.0045	1.28
Solvent	0.0%	0.0001	0.03
Solvent drying	0.8%	0.0075	2.14
Electrolyte	12.7%	0.0763	21.81
Total	100.0%	0.6012	171.78

[a] Costs are for cell construction only and do not include SEI formation step and pack assembly costs.

to Table 5 (or \$110.8 kW h^{-1}-usable energy). Using the baseline battery pack cost in Table 4 of \$514.6 kW h^{-1}-usable (or \$1.80 Ah^{-1} at an average cell voltage of 3.5 V), ***a pack cost savings of 21.5% is estimated for the processing improvements only***. It should be pointed out that certain processing tradeoffs required to implement aqueous processing and thick electrode coatings may affect these cost calculations to some degree. For example, dispersants and surfactants will likely be needed to prevent excessive agglomeration in water-based colloids, mixing times may be longer with certain water-soluble binders prior to coating, and drying protocols may need to be longer for thicker electrodes to ensure good adhesion of the coating to the current collector foil and agglomerate cohesion.

3. Wetting and formation cost calculations

3.1. Discussion of SEI layer formation steps

There is little public information available on the proprietary processes associated with LIB formation cycling, but there have been several recent studies attempting to gain scientific understanding of the SEI layer formation process, [37] SEI layer chemical and morphological characterization, [38–40] and its relationship to battery lifetime [41]. An informative review was published by Verma et al. where SEI layer properties and chemical compositions were compiled from other research groups' Fourier Transform Infrared Spectroscopy (FTIR) and X-ray Photoelectron Spectroscopy (XPS) results [42]. In general the SEI layer can be thought of as a bilayer structure whose morphology and composition is highly dependent on the charge–discharge process used during its formation, as well as a variety of electrolyte additives that are used to affect the structure and chemistry of the SEI. After formation cycling, this protective, passivating layer prevents the SEI layer from growing at a rapid rate and the anode graphite from further exfoliating. The bilayer structure that it is thought to take on consists of a primarily inorganic, crystalline inner layer (between the graphite particles and the outer portion of the SEI layer), which consists of compounds such as LiF, Li_2CO_3, Li_2O, $Li_2C_2O_4$, and LiOH. The outer portion of the SEI layer that interfaces with the liquid electrolyte is thought to be a mostly soft, organic polymer-like structure, consisting of compounds such as lithium ethylene dicarbonate (LiEDC), $ROCO_2Li$, ROLi, HCOLi, and polycarbonates [42]. Regardless of the actual variable composition, the SEI layer should remain electrically insulating, but highly conductive to Li ions. It should also promote quick solvation of Li ions into and de-solvation of Li ions from the solvent shells.

As for the electrolyte wetting and SEI formation steps used in industry, they are quite complex and interrelated. In general, the process takes 1.5–3 weeks (an unacceptable processing bottleneck and significant capital expense as tens of thousands of cyclers are needed to manage required throughput rates) and involves multiple wetting steps and charge–discharge cycles. Prior to wetting/aging and formation, the dry cells are filled with electrolyte. This step currently requires vacuum assist down to less than 25 mm Hg abs., which is an inherent sign of poor wetting of the electrolyte to the electrode materials (i.e. spontaneous wetting would require no vacuum assist). In addition, vacuum assisting will leave the smallest electrode pores void of electrolyte because the hydrodynamic forces are not enough to overcome the resistance of the capillary forces in a non-wetting situation.

Typically the formation process is started with an electrolyte wetting (i.e. aging) step above ambient temperature that lasts 2–3 days, followed by the first formation cycle (at extremely slow charging and discharging rates such as 0.05C/−0.05C). Next, another wetting step is completed for 1–2 days, followed by a faster formation cycle (such as 0.1C/−0.1C). The second wetting step is sometimes completed at elevated temperature (50–60 °C). A third formation cycle at even higher C rates (~0.25C/−0.25C) may be completed before the cell is charged to rated capacity and binned. In addition to the wetting and formation steps, the cell OCV must be checked along the way. The formation cycles themselves are often done above ambient temperature adding significantly to the cost of the process. Furthermore, the cells may need to warehoused (or incubated) after the first or second formation cycle, adding another processing bottleneck.

Each step in the wetting/formation-cycling process is critical to forming, in particular, the anode SEI layer. The electrolyte must be given adequate time to wet all electrode pore surface area (especially that at the mesopore level) before the first formation cycle can be completed. In order to maximize the amount of cathode lithium inventory that contributes to a structurally and chemically sound anode SEI layer, the first charge is typically done at extremely slow rates. Subsequent formation cycles can be completed at faster rates after the initial SEI layer is present. These second or third formation cycles are used to optimize the composition and morphology of the inner and outer portions of the SEI layer, and to allow electrolyte additives designed to build an SEI layer structure more suited for long cycle life. The periodic wetting steps allow for electrolyte (and additives) to wet still deeper into the smallest pores of the electrode before completing the next charge.

3.2. Formation baseline calculations

If it is assumed that circulating heated air at 50 °C is used to maintain temperature during initial electrode wetting, then the air supply would need to be constantly heated from 21 °C to 50 °C. If it is further assumed that the convective heat transfer coefficient of air to the cells of 100 W m^{-2} K^{-1} and a cell surface area of 0.101 m^2, then (100 W m^{-2} K^{-1}) (0.101 m^2) (29 °C) = 293 W for maintaining cell temperature would be needed. For a 48 h wetting period, that rate would correspond to (293 W) (48 h) = 14.1 kW h of energy. Since two separate wetting periods are usually required, 28.2 kW h would be needed for 96 h of total wetting time. For calculation simplicity, the same temperature for both wetting periods was used. If an efficiency of 95% is assumed for the input electricity to generate circulating heated air, then an electricity consumption of 29.7 kW h per 52-Ah cell for wetting alone.

For three (low-rate) formation cycles, three full charges and discharges plus a recharge at the end would be needed. If an average cell voltage of 3.5 V is assumed, then (52 Ah) (3.5 V) (7 half cycles) = 1.27 kW h for formation electricity consumption per cell is required. Therefore, a total of (29.7 + 1.27) kWh per 52-Ah cell is needed. Again, if an average cell voltage of 3.5 V is assumed, then (31.0 kW h electricity consumption)/((52 Ah) (3.5 V)/1000 kW h of energy storage) = 170 kW h kWh^{-1}.

In addition, the cells need to be heated slightly during the formation cycling (usually a lower air temperature than during wetting). If a cell heating temperature of 35 °C is needed during the formation cycles, the following additional convective air heating is required. Using the same heat transfer coefficient of 100 W m^{-2} K^{-1}, (100 W m^{-2} K^{-1}) (0.101 m^2) (14 °C) = 141 W is calculated. Three formation cycles at consecutive rates of C/20, C/10, and C/4 would take 68 h, so the heating requirement is (141 W) (68 h) = 9.6 kW h. Assuming a 95% efficiency of converting input electricity to heated air, 10.1 kW h for low-grade heating during formation cycling is required, or a total of (10.1 kW h electricity consumption)/((52 Ah) (3.5 V)/1000 kW h of energy storage)) = 55.5 kW h kWh^{-1}. Then the grand total for electricity consumption is (170 + 55.5) = 225.5 kW h kWh^{-1}. If the electricity cost is assumed to be \$0.10 per kWh, \$22.6 kW h^{-1} is the total cost

for formation cycling. This amount is 6.4% of the total pack cost (total energy basis) given in Table 4 of \$351.9 kW h^{-1}, which is quite substantial. If this time could be reduced by 60–75%, a pack level savings of \$13.6–17.0 kW h^{-1} could be realized (3.9–4.8% cost reduction on a total energy basis).

3.3. Possibilities for reducing wetting and formation-cycle costs

Wettability of the electrolyte to the electrode pores can be enhanced in two ways: 1) by supplying an additive to the electrolyte to lower its composite surface tension; and 2) by increasing the composite surface energy of the electrode. There is evidence that both of these approaches are effective. Active anode graphite has been modified through mild air oxidation to yield a high amount of surface oxygen groups. Capacity increased, irreversible capacity loss decreased, and cycling performance improved as a result of the oxidative treatment, which was mostly attributed to improved electrolyte wetting and formation of an SEI layer chemically bonded to the graphite surface oxygen groups [43]. Reeves and Morris modified the surface of a mesocarbon microbead (MCMB) anode to dramatically enhance wettability using a nonionic surfactant treatment, which improved the charging rate and cycle life. They also observed that both the electronic and charge-transfer resistance of the resulting SEI layer decreased [44].

When chloroethylene carbonate (CEC) was added in 20 vol% to an ionic liquid electrolyte mixture, charge transfer resistance was dramatically reduced and first-cycle efficiency (a direct indication of effective SEI formation) was dramatically increased in a natural graphite anode when compared to the same cell chemistry without this additive. This reduction was attributed to enhanced wettability and lower viscosity of the electrolyte mixture that contained the CEC additive [45].

Further evidence exists for significantly increasing the SEI-layer formation time, as shown by Märkle et al. [38]. In half cells using TIMCAL TIMREX® SFG44 graphite, the optimal formation current density varied significantly based on the electrolyte solvent used. Two different solvent solutions were evaluated: a 1:1 wt fraction of ethylene carbonate (EC)/dimethyl carbonate (DMC) and a 2:1 wt fraction of EC/propylene carbonate (PC). The major finding was that a C rate of ~0.9 (320 mA g^{-1} or ~1.25 mA cm^{-2}) gave the lowest first-cycle capacity loss and highest overall capacity for the EC/DMC case when compared to a range of lower currents. In contrast, a much lower C rate (~0.057, 20 mA g^{-1}, or ~78 μA cm^{-2}) was needed for the EC/PC case to obtain optimized first-cycle capacity loss. These findings were attributed to the fact that the solvent decomposition reaction kinetics were much faster than the solvent molecule co-intercalation kinetics with the combination of EC/DMC and the surface properties of the SFG44 graphite. For the EC/PC case, the PC solvent intercalation process was too fast regardless of charging rate, and a low current density was needed to obtain a morphology with minimum graphite exfoliation. The work of Märkle et al. highlights the balance between surface chemistry of the graphite anode, graphite morphology, electrolyte solvent chemistry, SEI-layer formation current density, and the possibility of electrolyte additives which further modify SEI layer chemistry.

Another possibility for reducing formation-cycle time is to systematically investigate completion of the first portions of the charging steps at much higher rates (~0.2C–0.5C) until the anode potential drops well below 1.0 V *vs.* Li/Li^+, the more critical potential range for forming an SEI layer with the required features for long cycle life. This change would result in the charging portion of the formation cycles being cut by well over half of the current time lengths (60–75%). Table 6 shows the combined cost reduction when considering aqueous processing, thick electrode, and reduced wetting/formation time (combination of fast charging to <1.0 V *vs.* Li/Li^+ and enhanced electrolyte wetting) advantages and should be compared to Table 4.

Table 6
LIB pack cost contributions for aqueous electrode processing with 2× electrode thickness and a 60–75% reduction in wetting and formation time (cost per kWh-usable energy assumes a 70% depth-of-discharge for cycling).

Cost component	Cost per kWh-total (\$/kWh)	Cost per kWh-usable (\$/kWh)
Composite electrode materials	100.2	143.1
Current collectors & separator	40.9	58.4
Electrode processing	2.2	3.1
Electrolyte	21.8	31.1
Wetting and formation cycling	7.5	10.7
Pouch and tab materials	6.7	9.6
Module hardware, power electronics & pack cooling [1]	46	65.7
Labor (electrode processing and cell/pack construction) [2]	34	48.6
Total	259.3	370.3

4. Comparison to published cost models

Our results are next compared to the two major PHEV battery pack cost studies that have been published recently by Argonne National Laboratory (ANL) [2] and TIAX, LLC [3]. The ANL cost model focuses mainly on P/E optimization and cost dependence, as well as pack design and cathode active material strategies for reducing costs, whereas this model focuses on production cost reduction strategies using current materials and manufacturing methods. In addition, the ANL cost model considers the capital investment of building a new LIB manufacturing plant to produce 100,000 LIB packs sized at 120 kg and 80 L for \$3400/pack. ANL's baseline pack design was based on 60 40-Ah pouch cells (50 kW and 8.7 kW h-total) with a maximum electrode thickness of 100 mm and a graphite/$LiNi_{0.8}Co_{0.15}Al_{0.05}O_2$ (NCA) cell chemistry. The projections were based on what it would cost to produce the batteries in 2020 at the pack-level energy density (72.5 Wh kg^{-1} and 109 W h L^{-1}) and power density (417 W kg^{-1} and 625 W L^{-1}) model targets. As for the cost of the baseline graphite/NCA cells, \$250 kW h^{-1}-total and \$357 kW h^{-1}-useable were calculated based on cell energy densities of 158 Wh kg^{-1} and 265 W h L^{-1}. For the graphite/$LiNi_{0.333}Mn_{0.333}Co_{0.333}O_2$ (NMC 333) case in the ANL model, \$258 kW h^{-1}-total and \$368 kW h^{-1}-useable were calculated at cell energy densities of 155 Wh kg^{-1} and 261 Wh L^{-1}, which provides a direct comparison to the results of this model. Fig. 1 shows a graphical summary of the baseline calculations and reduced costs (combination of aqueous processing, thick electrodes, and reduced wetting and formation time) from this work, and it is seen that this model yields graphite/NMC LIB pack costs somewhat higher than those of ANL, which is attributed to two factors: 1) the ANL model assumes 5–7 years of cell and manufacturing improvements and a more mature LIB supply chain between now and 2020; and 2) the ANL model does not fully account for the electrode processing and cell wetting/formation costs.

The TIAX model considered 5.5 kW h LIB PHEV packs with various cell chemistries with electrode areal capacity loadings of 1.5–3.0 mAh cm^{-2}. The cost for the graphite/NMC case in the TIAX model ranged from \$430–\$710 kW h^{-1}-usable (depending on the areal capacity loading) assuming 30% capacity fade and \$340–540 kW h^{-1} assuming 0% capacity fade. These results compare quite favorably with the results of this model (see Fig. 1). Interestingly, the TIAX model also found that 18–32% of ***cell*** manufacturing cost came from “aging and formation cycling”. For comparison, the same percentage for this model can be estimated using the baseline wetting/formation cost of \$44.1 kW h^{-1}-usable

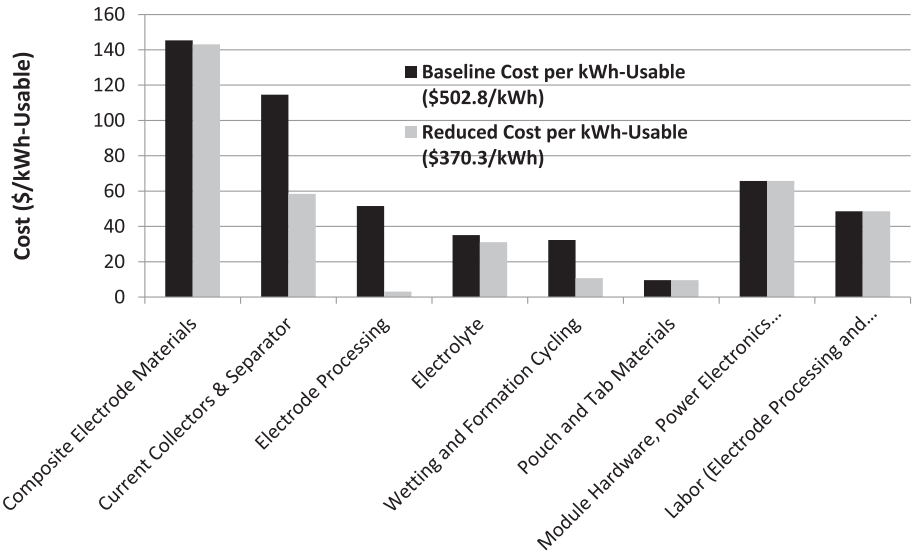

Fig. 1. Comparison of baseline and reduced pack costs (per kWh-usable basis) from ORNL model. "Reduced" cost is associated with implementing aqueous processing, thick electrode coatings, and reduced wetting and formation times (module hardware and labor costs taken from Refs. [1] and [2], respectively).

and the electrode processing cost of \$51.0 kW h^{-1}-usable. The cell formation fraction is then 46%, which is higher than the TIAX model. However, the TIAX model also includes winding, calendering, and electrode mixing costs, which this model does not. Therefore, the formation costs of this model and the TIAX model are in fairly good agreement.

5. Conclusions

A detailed processing cost breakdown was given for lithium-ion battery (LIB) electrodes, which focuses on the elimination of toxic, costly *N*-methylpyrrolidone (NMP) dispersion chemistry, doubling the thicknesses of the anode and cathode to raise energy density, and reduction of the anode electrolyte wetting and SEI-layer formation time. These benefits collectively offer the possibility of reducing LIB pack cost from \$502.8 kW h^{-1}-usable to \$370.3 kW h^{-1}-usable, a savings of \$132.5/kWh (or 26.4%). The technologies discussed here to achieve this cost reduction target are being researched and implemented at the DOE Battery Manufacturing and R&D Facility (BMF) at Oak Ridge National Laboratory (ORNL) and are generically adaptable to any anode or cathode cell chemistry (*i.e.* high voltage cathodes such as the lithium–manganese-rich NMC materials or high capacity anodes such as Si–C nanocomposite structures).

A step by step review of how these cost savings can be realized in existing or new LIB manufacturing plants is presented using a baseline case of thin (power) electrode thicknesses produced with NMP processing and a standard 10–14-day wetting and formation process. These results were compared to a thick (energy) electrode case with aqueous processing and a wetting and formation time reduced by 60–75%. It is shown that aqueous electrode processing can cut the electrode processing cost and energy consumption by an order of magnitude due to higher dispersion solids loading, lower drying temperature, lower air flow rate, and shorter drying time due to the lower boiling point, higher vapor pressure, and lower heat of vaporization of water. Doubling the thickness of the electrodes allows for using half of the inactive current collectors and separators, contributing even more cost savings than aqueous processing. In practice, these much thicker energy electrodes would need to be optimized for power performance using approaches such as multilayer electrode architectures, pore-size distribution gradients, and dual slot-die coating. Finally wetting and SEI-layer formation cost savings were discussed in the context of a protocol with significantly reduced time. Results of this cost contribution study were compared to those of the ANL and TIAX models. Excellent agreement in total LIB pack cost was found with respect to the TIAX model, which independently confirms their results by using a different cost constituent approach.

Acknowledgments

This research at Oak Ridge National Laboratory, managed by UT Battelle, LLC, for the U.S. Department of Energy (DOE) under contract DE-AC05-00OR22725, was sponsored by the Office of Energy Efficiency and Renewable Energy (EERE) Vehicle Technologies Office (VTO) (Program Manager: David Howell) Applied Battery Research subprogram (Program Manager: Peter Faguy). The authors would also like to thank Gabriel Veith, Andrew Payzant, Peter Faguy, and Jack Deppe for helpful technical discussions in finalizing the manuscript.

References

[1] D. Howell, Fiscal Year 2013 Annual Progress Report for Energy Storage R&D, U.S. Department of Energy, Office of Energy Efficiency and Renewable Energy, Vehicle Technologies Office, 2013, p. 2.
[2] K.G. Gallagher, D. Dees, P. Nelson, PHEV Battery Cost Assessment, in: DOE Annual Merit Review, May 9–13, 2011.
[3] B. Barnett, J. Rempel, C. McCoy, S. Dalton-Castor, S. Sriramulu, PHEV and LEESS Battery Cost Assessment, in: DOE Annual Merit Review, May 10, 2011.
[4] M.N. Rahaman, Ceramic Processing and Sintering, Marcel Dekker, Inc., New York, 1995.
[5] T.A. Ring, Fundamentals of Ceramic Powder Processing and Synthesis, Academic Press, San Diego, 1996.
[6] J.S. Reed, Principles of Ceramic Processing, second ed., John Wiley & Sons, Inc., New York, 1995.
[7] D.J. Shanefield, Organic Additives and Ceramic Processing, Kluwer Academic Publishers, Boston, 1995.
[8] R.J. Hunter, Foundations of Colloid Science, Oxford University Press, New York, 2001.
[9] G.H. Kirby, K.M. Cooley, B.L. Armstrong, ASME, Tailored rheological behavior of mullite and BSAS suspensions using a cationic polyelectrolyte, in: Proceedings of the ASME Turbo Expo2005, vol 1, 2005, pp. 307–313.
[10] J.H. Lee, J.-S. Kim, Y.C. Kim, D.S. Zang, U. Paik, Ultramicroscopy 108 (2008) 1256.
[11] J.H. Lee, J.-S. Kim, C. Kim, D.S. Zang, Y.-M. Choi, W.I. Park, U. Paik, Electrochem. Solid-State Lett. 11 (2008) A175.

[12] A. Guerfi, M. Kaneko, M. Petitclerc, M. Mori, K. Zaghib, J. Power Sources 163 (2007) 1047.
[13] C.-C. Li, J.T. Lee, C.-Y. Lo, M.-S. Wu, Electrochem. Solid-State Lett. 8 (2005) A509.
[14] C.-C. Li, J.T. Lee, X.W. Peng, J. Electrochem. Soc. 153 (2006) A809.
[15] C.-C. Li, J.T. Lee, Y.-L. Tung, C.-R. Yang, J. Mater. Sci. 42 (2007) 5773.
[16] Z.P. Cai, Y. Liang, W.S. Li, L.D. Xing, Y.H. Liao, J. Power Sources 189 (2009) 547.
[17] W. Porcher, B. Lestriez, S. Jouanneau, D. Guyomard, J. Electrochem. Soc. 156 (2009) A133.
[18] C.-C. Li, X.W. Peng, J.T. Lee, F.M. Wang, J. Electrochem. Soc. 157 (2010) A517.
[19] W. Porcher, B. Lestriez, S. Jouanneau, D. Guyomard, J. Power Sources 195 (2010) 2835.
[20] J.-T. Lee, Y.-J. Chu, F.-M. Wang, C.-R. Yang, C.-C. Li, J. Mater. Sci. 42 (2007) 10118.
[21] J.-T. Lee, Y.-J. Chu, X.-W. Peng, F.-M. Wang, C.-R. Yang, C.-C. Li, J. Power Sources 173 (2007) 985.
[22] J. Li, B.L. Armstrong, J. Kiggans, C. Daniel, D.L. Wood III, J. Electrochem. Soc. 160 (2013) A201.
[23] J. Li, B. Armstrong, J. Kiggans, C. Daniel, D.L. Wood III, Langmuir 28 (2012) 3783.
[24] J. Li, C. Rulison, J. Kiggans, C. Daniel, D.L. Wood III, J. Electrochem. Soc. 159 (2012) A1152.
[25] J. Li, B.L. Armstrong, J. Kiggans, C. Daniel, D.L. Wood, J. Colloid Interface Sci. 405 (2013) 118.
[26] B.L. Armstrong, C. Daniel, D.L. Wood, and J. Li, "Aqueous Processing of Composite Lithium Ion Electrode Material," Filed October 12th, 2012, U.S. Patent Application No. 13/651,270, Publication No. US20130108776 A1 (UT-Battelle, LLC).
[27] D.L. Wood III, Overcoming Processing Cost Barriers of High-performance Lithium-ion Battery Electrodes, in: DOE Annual Merit Review, May 13-17, 2013.
[28] P. Arora, R.E. White, J. Electrochem. Soc. 145 (1998) 3647.
[29] S. Zhang, M.S. Ding, K. Xu, J. Allen, T.R. Jow, Electrochem. Solid State Lett. 4 (2001) A206.
[30] R. Fong, U. von Sacken, J.R. Dahn, J. Electrochem. Soc. 137 (1990) 2009.
[31] P.C.J. Chiang, M.S. Wu, J.C. Lin, Electrochem. Solid State Lett. 8 (2005) A423.
[32] J. Li, E. Murphy, J. Winnick, P.A. Kohl, J. Power Sources 102 (2001) 302.
[33] J. Vetter, P. Novák, M.R. Wagner, C. Veit, K.C. Möller, J.O. Besenhard, M. Winter, M. Wohlfahrt-Mehrens, C. Vogler, A. Hammouche, J. Power Sources 147 (2005) 269.
[34] S.-Y. Yoon, R. Iocco, U.S. Patent Application 12/558,091 (A123 Systems, Inc.), 2010.
[35] S.S. Kim, J.C. Hyun, Drying of coated film, in: George Wypych (Ed.), Handbook of Solvents, ChemTec Publishing, Toronto, Canada, 2001, pp. 396–399.
[36] C.J. Geankoplis, in: Transport Processes and Unit Operations, second ed., Allyn and Bacon, Inc., Boston, 1983, p. 502.
[37] M.B. Pinson, M.Z. Bazant, J. Electrochem. Soc. 160 (2013) A243.
[38] W. Märkle, C.-Y. Lu, P. Novák, J. Electrochem. Soc. 158 (2011) A1478.
[39] P. Lu, C. Li, E.W. Schneider, S.J. Harris, J. Phys. Chem. C. 118 (2014) 896.
[40] A. Tokranov, B.W. Sheldon, P. Lu, X. Xiao, A. Mukhopadhyay, J. Electrochem. Soc. 161 (2014) A58.
[41] C. Huang, K. Huang, H. Wang, S. Liu, Y. Zeng, J. Solid State Electrochem. 15 (2011) 1987.
[42] P. Verma, P. Maire, P. Novák, Electrochim. Acta 55 (2010) 6332.
[43] E. Peled, D. Golodnitsky, SEI on lithium, graphite, disordered carbons and tin-based alloys, in: P.B. Balbuena, Y. Wang (Eds.), Lithium-ion Batteries: Solid-electrolyte Interphase, Imperial College Press, London, 2004, pp. 49–50.
[44] S.D. Reeves, R.S. Morris, Electrochem. Solid State Lett. 7 (2004) B29.
[45] H. Zheng, K. Jiang, T. Abe, Z. Ogumi, Carbon 44 (2006) 203.